Extensive chaos in the Lorenz-96 model

Cite as: Chaos **20**, 043105 (2010); https://doi.org/10.1063/1.3496397
Submitted: 02 April 2010 • Accepted: 13 September 2010 • Published Online: 02 November 2010

A. Karimi and M. R. Paul

Extensive chaos in the Lorenz-96 model

A. Karimi[1] and M. R. Paul[2,a)]
[1]*Department of Engineering Science and Mechanics, Virginia Polytechnic Institute and State University, Blacksburg, Virginia 24061, USA*
[2]*Department of Mechanical Engineering, Virginia Polytechnic Institute and State University, Blacksburg, Virginia 24061, USA*

(Received 2 April 2010; accepted 13 September 2010; published online 2 November 2010)

We explore the high-dimensional chaotic dynamics of the Lorenz-96 model by computing the variation of the fractal dimension with system parameters. The Lorenz-96 model is a continuous in time and discrete in space model first proposed by Lorenz to study fundamental issues regarding the forecasting of spatially extended chaotic systems such as the atmosphere. First, we explore the spatiotemporal chaos limit by increasing the system size while holding the magnitude of the external forcing constant. Second, we explore the strong driving limit by increasing the external forcing while holding the system size fixed. As the system size is increased for small values of the forcing we find dynamical states that alternate between periodic and chaotic dynamics. The windows of chaos are extensive, on average, with relative deviations from extensivity on the order of 20%. For intermediate values of the forcing we find chaotic dynamics for all system sizes past a critical value. The fractal dimension exhibits a maximum deviation from extensivity on the order of 5% for small changes in system size and the deviation from extensivity decreases nonmonotonically with increasing system size. The length scale describing the deviations from extensivity is consistent with the natural chaotic length scale in support of the suggestion that deviations from extensivity are due to the addition of chaotic degrees of freedom as the system size is increased. We find that each wavelength of the deviation from extensive chaos contains on the order of two chaotic degrees of freedom. As the forcing is increased, at constant system size, the dimension density grows monotonically and saturates at a value less than unity. We use this to quantify the decreasing size of chaotic degrees of freedom with increased forcing which we compare with spatial features of the patterns. © *2010 American Institute of Physics*. [doi:10.1063/1.3496397]

We explore fundamental questions regarding the composition and description of spatiotemporal chaos in high-dimensional systems. The Lorenz-96 model is used for its phenomenological relevance to fluid convection and atmospheric dynamics. We compute the variation of the fractal dimension over a wide range of system parameters, for very long-times, and over many initial conditions. We explore two limits: the "spatiotemporal chaos" limit where the system size is increased while holding the external forcing constant and the "strong driving" limit where the external forcing is increased for a system of fixed size. The variations in the fractal dimension with system parameters are used to provide estimates for characteristic length and time scales describing the chaotic dynamics. These findings are directly compared with experimentally accessible diagnostics of the pattern dynamics to provide new physical insights into the underlying features of high-dimensional chaos.

I. INTRODUCTION

A common feature of spatially extended systems that are driven far-from-equilibrium is spatiotemporal chaos where the dynamics are aperiodic in space and time.[1] Important examples include the dynamics of the atmosphere and climate,[2] fluid convection,[1,3] the convection of biological organisms in the oceans,[4] the transition to chaos in excitable media,[5] and the complicated dynamics of systems of reacting, advecting, and diffusing chemicals.[6] Despite intense theoretical and experimental investigation many important challenges remain regarding how to characterize, control, and predict the dynamics of these large complex systems.

A unifying feature of many of these systems is that the dimension of the attractors describing their dynamics in phase space is very large. This severely limits the use of sophisticated techniques of chaotic time-series analysis[7] and of powerful geometry based descriptions of dynamical systems.[8] However, the use of Lyapunov exponents to compute the fractal dimension does not suffer from these limitations and provides an important window into fundamental aspects of the dynamics of high-dimensional chaotic systems. Furthermore, the spectrum of Lyapunov exponents is inaccessible to experimental measurement using currently available techniques which leaves their numerical computation as an important way to gain new insights. A physical understanding of the dimension and how it varies with system parameters can provide fundamental knowledge regarding the underlying nature of spatiotemporal chaos that can be used to guide the development of improved theoretical descriptions for experimentally accessible systems.

a)Electronic mail: mrp@vt.edu.

A defining feature of chaos is the sensitive dependence of the system dynamics on initial conditions and the exponential separation of nearby trajectories in phase space.[9] The rate of separation is quantified by the spectrum of Lyapunov exponents λ_i, where $i=1,\ldots,N$ with λ_i arranged in descending order and N is the total number of degrees of freedom in the system. For partial differential equations, although the phase space is infinite, the value of N is expected to be very large but finite corresponding to the dimension of the inertial manifold (cf. Refs. 10 and 11). For a system of coupled ordinary differential equations, as we study here, the value of N is equal to the number of independent variables. The summation of the first M exponents (where $M \leq N$) describes the growth of an M-dimensional ball of initial conditions in N-dimensional phase space. The number of exponents required for the sum to vanish is the dimension of the ball that will neither grow nor shrink and is an estimate of the fractal dimension D_λ of the strange attractor. Using a linear interpolation to determine the number of exponents yields the well-known Kaplan–Yorke formula,

$$D_\lambda = K + \sum_{i=1}^{K} \frac{\lambda_i}{|\lambda_{K+1}|}, \tag{1}$$

where K is the largest integer such that the sum of the first K Lyapunov exponents is non-negative.[12] The magnitude of D_λ is an approximate value of the number of degrees of freedom acting in the system.[13,14]

Ruelle[15] initially conjectured, and numerical simulation later confirmed (cf. Refs. 16 and 17), that the fractal dimension is extensive for large chaotic systems. More precisely, D_λ increases linearly with the volume of the system L^d, where L is a characteristic length and d is the number of spatially extended dimensions. The extensivity of D_λ is a consequence of spatial disorder. If two subsystems are sufficiently far apart their coupling is weak and they contribute independently and additively to the overall dimension.[1,13] Cross and Hohenberg[1] used this to define a natural chaotic length scale as

$$\xi_\delta = \left(\frac{D_\lambda}{L^d}\right)^{-1/d}, \tag{2}$$

where a volume ξ_δ^d will contain, on average, one degree of freedom.

Using the above arguments, one intriguing possibility is that underlying spatiotemporal chaos are structures of volume $\sim \xi_\delta^d$. This raises an interesting question: How does the dimension vary for changes in system volume that are smaller than ξ_δ^d? One possibility is that D_λ is proportional to the system size only on average. In this case, the variation of D_λ would have a stepwise structure with system size where the steps correspond to the addition of new degrees of freedom as the system grows large enough to accommodate them. A smoother transition may also be possible where the new degrees of freedom are able to stretch or compress to match the system size. In light of this, the variation of D_λ for small changes in system size can shed important physical insight upon the basic nature and composition of spatiotemporal chaos (cf. Refs. 1 and 18–20).

Questions relating to the precise variation of the fractal dimension with system size have been explored numerically for several important model equations. O'Hern *et al.*[16] explored the extensive chaos of a two-dimensional coupled-map lattice with an Ising-like transition. The fractal dimension was found to exhibit significant deviations from extensivity near the onset of spatiotemporal chaos which rapidly decayed with increasing system size (here the number of lattice sites).

Xi *et al.*[20] explored the one-dimensional (1D) Nikolaevskii equation and Tajima and Greenside[19] explored the 1D Kuramoto–Sivashinsky equation. In both of these studies extensive chaos was found and a systematic exploration of the dimension was performed in the extensive regime. The fractal dimension remained linear to within the precision of the calculations to yield what is now referred to as microextensive chaos. It is important to note that neither study focused upon the approach to extensive chaos where deviations may be more accessible. At the larger system sizes explored it remains a possibility that deviations in the fractal dimension were too small to detect.

Fishman and Egolf[18] explored the 1D complex Ginzburg–Landau equation over a range of system sizes including the approach to extensive chaos. Significant deviations from extensivity were found to occur on a length scale consistent with ξ_δ, which was used to suggest the presence of building blocks that compose spatiotemporal chaos.[18]

Computations of the fractal dimension have also been conducted for experimentally accessible systems such as Rayleigh–Bénard convection (the buoyant convection that occurs in a shallow fluid layer heated from below). Extensive chaos was found in large periodic boxes[21] and in finite cylindrical domains[22] yielding a natural chaotic length scale $\xi_\delta \approx 2$ corresponding approximately to the width of a convection roll pair. However, such calculations are very expensive and it remains unclear if a fluid system such as Rayleigh–Bénard convection is microextensive.

The approach we take is to study the dynamics of a periodic lattice of coupled variables (discrete in space and continuous in time) whose equations of motion were originally developed by Lorenz in 1996 with the dynamics of the atmosphere and fluid convection in mind.[23] The model has since become important in the study of forecasting spatiotemporally chaotic systems. The model is now known as the Lorenz-96 model and is described in detail below. We compute the spectrum of Lyapunov exponents and fractal dimension using standard approaches. The contribution of this paper is a systematic and careful study of the variations in the fractal dimension with changes in system parameters to gain physical insights into high-dimensional chaos. By exploring a simple model we are able to perform very long-time simulations, over many initial conditions, and for a broad range of system parameters.

II. THE LORENZ-96 MODEL

The Lorenz-96 model is a simple model developed by Lorenz in 1996 to study difficult questions regarding predictability in weather forecasting.[23] The model is constructed of variables that represent the continuous time variation of an

atmospheric quantity of interest, such as temperature or vorticity, at a discrete location on a periodic lattice representing a latitude circle on the earth. The discrete variables are coupled spatially and their equation of motion includes contributions relevant to fluid systems including a quadratic nonlinearity, dissipation, and a constant external forcing. However, the equations are phenomenological and cannot be derived systematically from a more rigorous description.

Despite these simplifications the Lorenz-96 model has emerged as an important and often used model system for the testing of new ideas in the atmospheric sciences[24–26] and in the general study of spatiotemporal chaos.[27] In our work, we explore the Lorenz-96 model as a numerically accessible model with phenomenological relevance to fluid systems. The computational cost of a systematic study of the variation of the fractal dimension with system parameters is significant. It is anticipated that our exploration of a simple model will yield new insights that can be used to guide future studies of more complicated systems.

Mathematically, the Lorenz-96 model is a linear lattice of N variables where the dynamics of the kth variable is given by

$$\frac{dX_k}{dt} = (X_{k+1} - X_{k-2})X_{k-1} - X_k + F \tag{3}$$

for $k=1,\ldots,N$. In this equation F represents an external driving, $-X_k$ is a damping term, and the quadratic term is an advection term that has been constructed to conserve kinetic energy (represented as the sums of squares of X_k) in the absence of damping. We consider the case of constant external forcing F and where the lattice is periodic in space. Although other boundary conditions are possible, periodic boundaries are of particular relevance for the atmospheric systems of which this model was intended to describe. We will show that the chaotic and periodic solutions we explore are composed of traveling structures that travel completely around the periodic lattice many thousands of times. In light of this, other boundary conditions such as an absorbing boundary would have a very strong impact on the dynamics. We have not explored these possibilities in detail.

The two parameters N and F completely determine the dynamics. The value of N is the system size and F is the magnitude of the external forcing. In the following we are interested in the variation of the fractal dimension with these parameters. We explore system sizes $N \geq 4$ since $N=3$ does not yield interesting dynamics due to the nature of the coupling. For small values of the forcing $F < 8/9$ it has been shown[24] that all solutions decay to the steady solution $X_k = F$.

We compute the spectrum of Lyapunov exponents λ_k and the fractal dimension D_λ using the standard procedure described in detail in Ref. 28. There are N exponents and for each exponent a set of equations linearized about Eq. (3) is evolved simultaneously to yield the dynamics of perturbations arbitrarily close to the full nonlinear system. These tangent space equations are

$$\frac{d\delta X_k^{(i)}}{dt} = X_{k-1}\delta X_{k+1}^{(i)} + (X_{k+1} - X_{k-2})\delta X_{k-1}^{(i)} - X_{k-1}\delta X_{k-2}^{(i)} - \delta X_k^{(i)}, \tag{4}$$

where $\delta X_k^{(i)}$ is the ith perturbation about lattice site k and $i = 1,\ldots,N$. The perturbations are reorthonormalized using a Gram–Schmidt procedure after a time t_N to yield the magnitude of their growth $\|\delta X_k^{(i)}(t_N)\|$. Each reorthonormalization yields a value of the instantaneous Lyapunov exponent,

$$\tilde{\lambda}_k = \frac{1}{t_N}\ln\|\delta X_k^{(i)}\|. \tag{5}$$

This is repeated and the average value of $\tilde{\lambda}_k$ yields the finite time Lyapunov exponent,

$$\lambda_k = \frac{1}{N_t}\sum_{i=1}^{N_t}\tilde{\lambda}_k, \tag{6}$$

where N_t is the number of reorthonormalizations performed. The limit $N_t \to \infty$ yields the infinite-time Lyapunov exponent.

In our numerical simulations, we begin from random initial conditions and use a fourth-order Runge–Kutta time integration with a time step $\Delta t = 1/64$. Typically, we integrate forward for 1000 time units before starting the calculation of Lyapunov exponents to ensure that all transients have decayed. At this point we begin integrating the tangent space equations using $t_N = 1$. All of our reported results are for very long simulation times $t \gtrsim 5 \times 10^5$ and we have computed results for each set of parameter values for 10–50 different random initial conditions.

III. RESULTS

A. The variation of the fractal dimension with system size

1. Small external forcing, F=5

We first explore the dynamics for a small value of the forcing term $F=5$ over a wide range of system sizes, $4 \leq N \leq 50$. We find that the dynamics are characterized by windows of periodic and chaotic behavior. Figure 1 shows space-time plots for $X_k(t)$ illustrating the variety of dynamics present. In Fig. 1(a) the dynamics are periodic for $N=38$ yielding a wave of constant velocity traveling from right to left. In Fig. 1(b) we show the interesting case $N=22$ where the dynamics are chaotic with a small value of the fractal dimension. The dynamics consist of a distorted wave structure traveling from right to left. In Fig. 1(c) chaotic dynamics are shown for $N=47$. This illustrates the typical chaotic dynamics that we have observed where the traveling wave structure is still apparent but with significant distortions and deviations.

It is evident from these space-time plots that the time for a wave structure to travel completely around the periodic lattice ring is ~ 10 time units for sizes of the lattice rings used here. Our typical simulation time is on the order of 10^5 time units which indicates that the number of complete rotations in one of our simulations is approximately 10^4. The very long simulation times were required to gather statistics

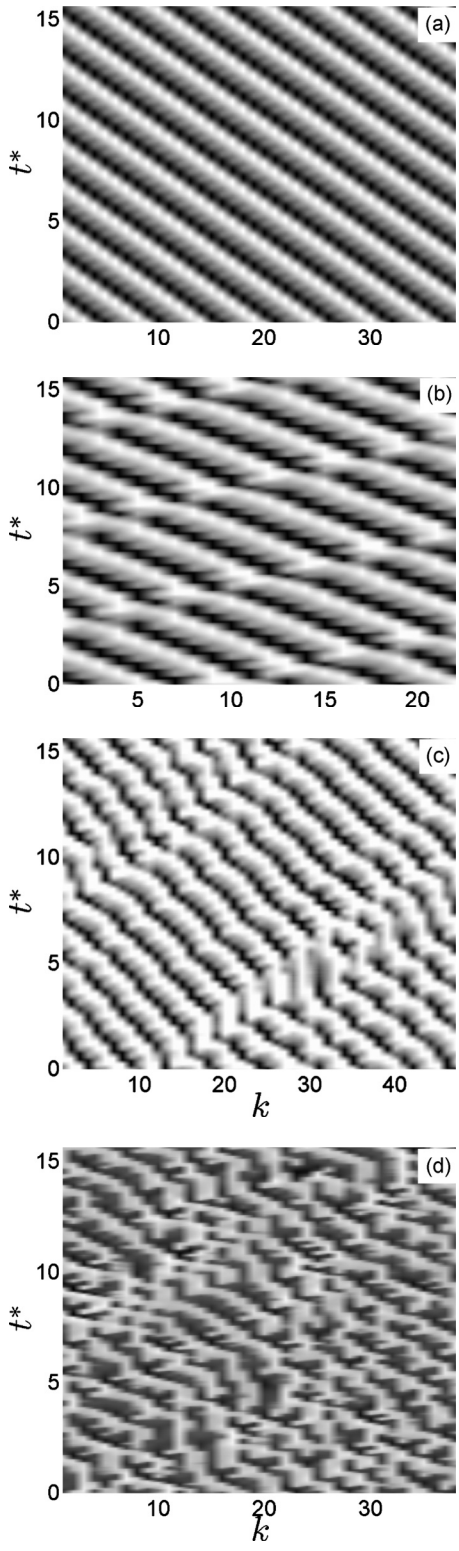

FIG. 1. Space-time plots of $X_k(t)$ for 15 time units after $t=5.1\times10^5$ indicated by t^*. Dark regions are large values and light regions are small values: (a) $N=38$, $F=5$, periodic dynamics; (b) $N=22$, $F=5$, low-dimensional chaotic dynamics; (c) $N=47$, $F=5$, chaotic dynamics; (d) $N=38$, $F=10$, chaotic dynamics.

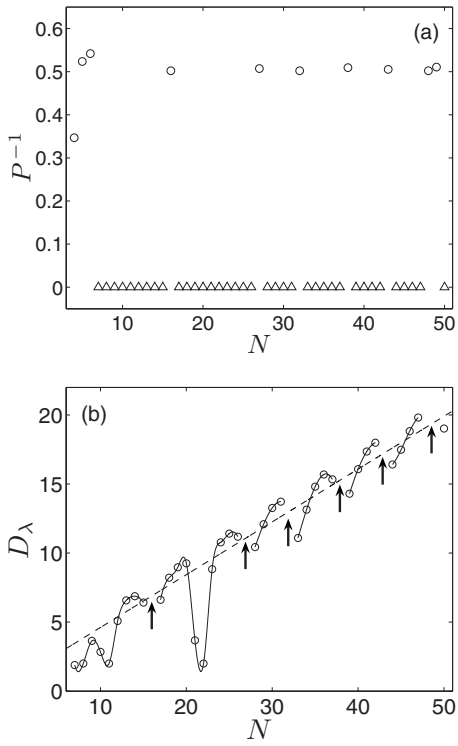

FIG. 2. The variation of the dynamics with system size N for $F=5$. (a) The variation of the inverse of the period P of the dynamics with system size N where circles are periodic dynamics and triangles are chaotic dynamics. (b) Deviations from extensivity illustrated by the variation of D_λ with N. The circles are simulation results and the solid lines are to guide the eye. The maximum value of $\Delta D=0.77$ occurs for $N=22$, for $N\geq27$ the maximum deviation is $\Delta D=0.17$, where ΔD is computed using Eq. (7). The arrows indicate windows of periodic dynamics. The error in these calculations is $\sim10^{-2}$ as determined by the standard deviation of D_λ using ten different initial conditions at each N.

with sufficient accuracy to address many of the subtle questions we study. Despite the simple nature of the model studied the requirement for very long-time simulations is significant. Overall, this suggests that the slow and noisy nature of the convergence of the Lyapunov spectrum can pose significant computational challenges for more complicated models.

Figure 2(a) illustrates the variation in dynamics with system size where P^{-1} is the inverse period of the dynamics. The circles represent system sizes yielding periodic dynamics. For systems $N\geq5$ the period of oscillation is approximately 2 time units. The triangles, located at $P^{-1}=0$, represent system sizes that yield chaotic dynamics. For each system size N we performed ten long-time numerical simulations starting from different random initial conditions. The type of dynamics found was independent of the initial conditions used.

Figure 2(b) shows the variation of D_λ with system size N. The circles represent the fractal dimension for system sizes yielding chaos and the solid line is to guide the eye. The error in D_λ at each value of N is $\sim10^{-2}$ as determined by the standard deviation in the fractal dimension from simulations initiated with ten different initial conditions. The dashed line is a linear curve fit through the data for $N\geq27$ to yield an estimate of D_{ext} describing the dimension of extensive chaos. In all of our calculations of D_λ we use a third order polynomial curve fit to determine an accurate value for the number of Lyapunov exponents that must be included for the sum to vanish (the curve fit uses only the four sums with values closest to zero).[18] The arrows highlight the gaps be-

TABLE I. Characteristic length scales describing the dynamics: (first row) $F=5$, (second row) $F=10$. ξ_δ is the chaotic length scale found using the fractal dimension, ξ_0 is the average wavelength of the deviations in the fractal dimension about extensivity, and ξ_L is the average wavelength of the wave structure. ξ_0/ξ_δ is an estimate for the number of chaotic degrees of freedom per wavelength of the deviation from extensivity, ξ_L/ξ_δ is an estimate for the number of chaotic degrees of freedom per wavelength of the pattern. The results for $F=10$ are for the large system limit $N\geq 40$.

	ξ_δ	ξ_0	ξ_L	ξ_0/ξ_δ	ξ_L/ξ_δ
$F=5$	2.6	5.7	5.2	2.2	2.0
$F=10$	1.35	2.1	4.45	1.5	3.3

tween chaotic dynamics indicating system sizes yielding periodic dynamics. Using the slope of the dashed line of Fig. 2(b) and Eq. (2) the chaotic length scale is $\xi_\delta=2.6$. For reference, the characteristic lengths determined from our calculations are collected in Table I.

The size of the windows of chaotic dynamics is largest for the smaller system sizes. For $N\geq 27$ the dynamics alternate between chaotic and periodic dynamics in a regular manner. The size of the interval between periodic dynamics yields a length scale we will denote by ξ_p. For $N\geq 27$ there are four such intervals with an average value of $\xi_p=5.25$. This yields $\xi_p/\xi_\delta=2.0$ indicating the presence of two chaotic degrees of freedom contained in each interval between periodic dynamics. This suggests that the periodic dynamics occur when the system size has been increased sufficiently enough to accommodate two additional degrees of freedom. System sizes larger or smaller than this value yield chaotic dynamics in agreement with what was found for the 1D complex Ginzburg–Landau equation.[18]

To quantify the deviations of the dimension from purely extensive chaos we define

$$\Delta D = \frac{D - D_{\text{ext}}}{D_{\text{ext}}}. \tag{7}$$

The overall maximum value of the deviation from extensivity occurs for $N=22$ where $\Delta D=0.77$. If one only considers $N\geq 27$ the maximum deviation is $\Delta D=0.17$. To estimate the error in these calculations we computed results at each value of N using ten different random initial conditions. The standard deviation of the values of D_λ is $\lesssim 10^{-2}$, which is too small to include as error bars in Fig. 2(b). The deviations from extensivity exhibit regular variations about the line of purely extensive chaos for $N\geq 25$. To quantify the length scale of these deviations we used a cubic spline interpolation through the data symbols (shown as the solid line) to determine the average wavelength of these deviations which we will denote as ξ_0. Using this approach yields a value of $\xi_0=5.7$. The ratio $\xi_0/\xi_\delta=2.2$ yields that there are, on average, 2.2 chaotic degrees of freedom per wavelength of the deviation from extensive chaos. This is consistent with what has also been observed for the complex Ginzburg–Landau equation.[18]

We now compare these results based upon the use of Lyapunov exponents with what is found by analyzing the spatial and temporal characteristics of the patterns. Analysis of the patterns is of particular interest because these measurements are often available in experiment whereas the Lyapunov exponent based diagnostics are not. Figure 3(a) shows the variation of the correlation time ξ_t with increasing system size. The correlation time is computed from

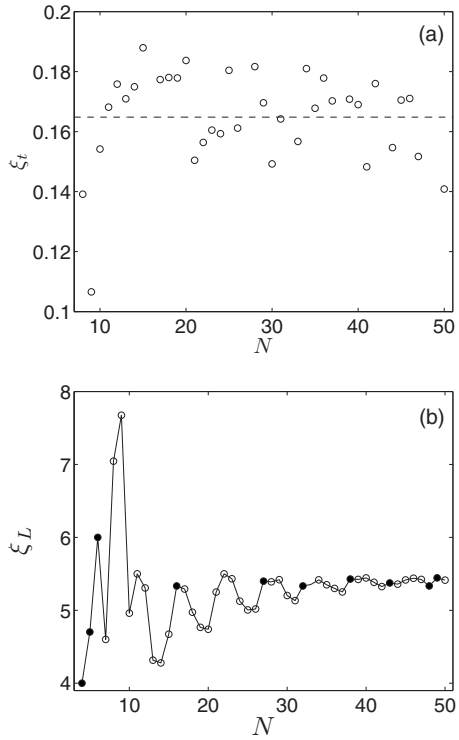

FIG. 3. The temporal and spatial features of the patterns for $F=5$. (a) The variation of the average correlation time ξ_t with system size N. The dashed line is the average value of ξ_t. (b) The variation of the pattern wavelength ξ_L with system size. Open symbols represent chaotic dynamics and filled symbols represent periodic dynamics.

$$\langle \bar{X}_k(0)\bar{X}_k(t)\rangle \sim e^{-t/\xi_t}, \tag{8}$$

where $\langle \bar{X}_k(0)\bar{X}_k(t)\rangle$ is the autocorrelation of the kth variable $\bar{X}_k$ in which we have subtracted off the mean value. The results shown are the time average value of the correlation time for the variable $\bar{X}_1(t)$ in the periodic lattice. Each data point is also averaged over simulations which begun from ten different random initial conditions. The results exhibit a scatter about the mean value of $\xi_t=0.162$ with a coefficient of variation of 9.6% (defined as the standard deviation divided by the mean). The results indicate that the time dynamics remain relatively constant as the system size increases.

To quantify the spatial variation of the pattern we have computed the average pattern wavelength ξ_L with increasing system size, as illustrated in Fig. 3(b). The wavelength is computed in Fourier space using the location of the largest peak at small wavenumber to capture the size of the basic wave structure and is averaged over all time for each initial condition. For smaller systems $N\lesssim 10$ the deviations are largest, whereas for $N>10$ the wavelength varies about an average value of $\xi_L\approx 5.2$ lattice spacings. For the chaotic solutions, the fluctuations about the average value over the ten different initial conditions yield a coefficient of variation of approximately 14%. For the periodic dynamics the wavelength of the periodic states was nearly identical to the pre-

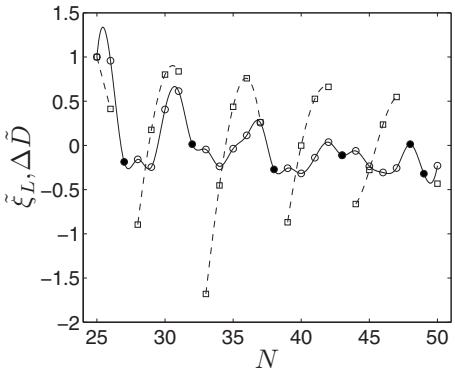

FIG. 4. A comparison of the variation in the normalized pattern wavelength $\tilde{\xi}_L$ and the normalized deviation from extensivity $\Delta\tilde{D}$ for $F=5$ and $N\geq 25$. The constant normalization factors are chosen such that $\Delta\tilde{D}$ and $\tilde{\xi}_L$ each equal unity for $N=25$ allowing both curves to fit on a single plot. The wavelength results are given by the circles and the solid line (open symbols are chaotic dynamics, filled symbols are periodic dynamics). The deviations from extensivity are shown by the square symbols and the dashed line where gaps indicate regions of periodic solutions. In both cases the lines are to guide the eye.

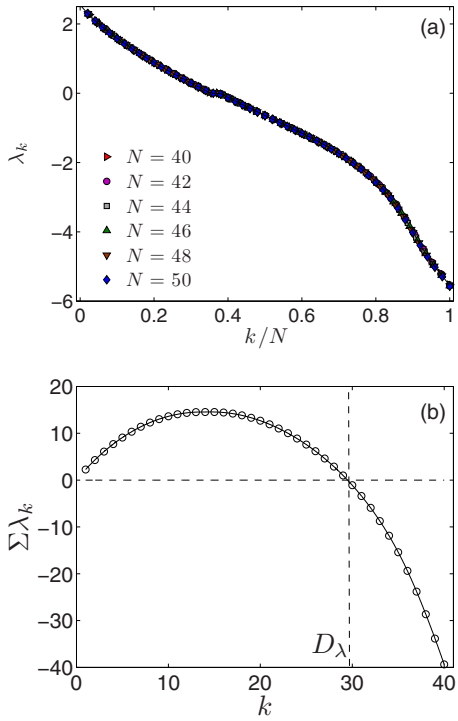

FIG. 5. (Color online) (a) The variation of the Lyapunov exponents λ_k with k/N for $k=1,\ldots,N$, where N is the system size and $F=10$. The solid line is the average value using all of the data. (b) The variation of the summation of the exponents with k for $F=10$ and $N=40$. The fractal dimension D_λ is the value where the summation vanishes. The solid line is a sixth order polynomial curve fit and the fractal dimension D_λ is shown by the vertical dashed line.

cision of our calculations over the different initial conditions. Computation of the two-point spatial correlation length is difficult due to the lack of an exponential decay in the correlation functions for the parameters we have explored and is not included.

Our space-time diagnostics indicate that with increasing system size the dynamics tend toward a state where $\xi_t \approx 0.16$ and $\xi_L \approx 5.2$. The wavelength of the pattern in the large system limit is $\xi_L \approx 0.9\xi_0 \approx 2\xi_\delta$, indicating that each wavelength of the pattern contains approximately two chaotic degrees of freedom on average. In this case, it is useful to also compare the deviations from extensivity with the variations in the wavelength of the patterns for increasing system size.

The variation of ξ_L about its mean value is quite similar to what is found for the deviations from extensivity ΔD and is illustrated in Fig. 4. We plot the variation of the normalized wavelength $\tilde{\xi}_L$ and the normalized deviations from extensivity $\Delta\tilde{D}$ with the system size. The constant normalization factors are chosen such that the normalized wavelength and deviation from extensivity equal unity for $N=25$, allowing both curves to be shown on a single plot. The circles are results for the wavelength of the pattern where solid symbols indicate periodic dynamics, and open symbols represent chaotic dynamics. The dashed line and the square symbols represent the deviations from extensivity. Gaps in the dashed line occur for system sizes exhibiting periodic dynamics.

Figure 4 illustrates a correlation between the pattern wavelength and the deviation from extensivity. The general trend is that both the fractal dimension and the pattern wavelength increase with increasing system size until the pattern adjusts by adding an additional wave structure to the periodic lattice effectively reducing the average wavelength of the pattern. With the addition of the wave structure the dynamics are periodic and the fractal dimension vanishes. A similar trend is seen in the work of Fishman and Egolf,[18] where periodic dynamics were found for system sizes where the deviation from extensivity was predicted to be a minimum for the one-dimensional complex Ginzburg–Landau equation.

2. Intermediate external forcing, $F=10$

We next explore the dynamics for a larger value of the forcing $F=10$ over the range of system sizes $5\leq N\leq 50$. For each system size we have performed 50 independent numerical simulations starting from different random initial conditions. Each simulation was allowed to continue until $t=5\times 10^5$ and in computing our results we only used data in the time interval $3\times 10^5 \leq t \leq 5\times 10^5$ to ensure the decay of all transients and in order to gather good statistics. We found chaotic dynamics at every system size and for each random initial condition. A representative space-time plot for our results is shown in Fig. 1(d) for the case of $N=38$. The patterns consist of distorted wave structures traveling from right to left.

The spectra of Lyapunov exponents are shown in Fig. 5(a) for six different values of system size. The spectra collapse onto a single curve as expected for extensive chaos. The solid line is the average of the results for the different system sizes shown. The variation of the summation of the exponents with the number of exponents is illustrated in Fig. 5(b) for the case of $N=40$. The solid line is a sixth order polynomial curve fit through the data. The fractal dimension is indicated by the vertical dashed line at the location where the summation vanishes.

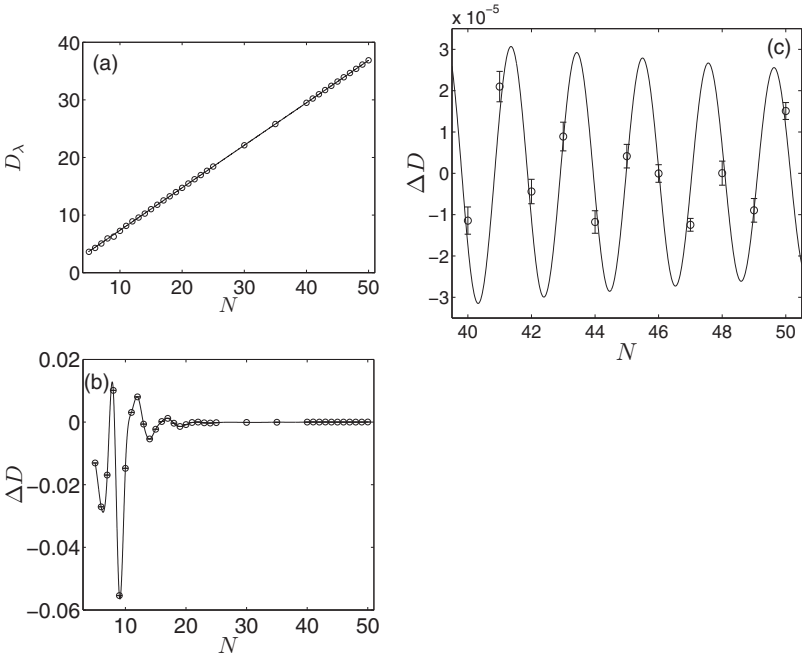

FIG. 6. The variation of the dynamics with the system size for $F=10$. (a) The variation of D_λ with N, the solid line is a linear curve fit through the data indicating extensive chaos. For $N=4$ the dynamics are periodic and are not included in the curve fit. (b) The variation of the deviation from extensivity ΔD with N. The circles are results from numerical simulation and the solid line is a spline interpolation to guide the eye. The deviations from extensivity are on the order of 5% and decrease with increasing N. (c) A close-up view illustrating the deviations from extensivity for large N. The solid line is a curve fit given by $\Delta D=1.3\times10^{-3}N^{-1}\cos(2\pi N/\xi_0)$ where the wavelength $\xi_0=2.1$ lattice spacings. The error bars shown in (b) and (c) are on the order of $\sim10^{-5}$ and $\sim10^{-6}$, respectively, and are computed from the standard deviation of the fluctuations of D_λ about its average value using simulations from 50 different initial conditions.

The variation of the fractal dimension with system size is shown in Fig. 6. Figure 6(a) illustrates the variation of D_λ with N where the symbols represent the average value over the 50 different initial conditions. An estimate of the error in these calculations is the standard deviation of the values of the dimension at each system size. Using this, the error is found to be quite small with a magnitude that is $\lesssim10^{-5}$ over the entire range of system sizes. The solid line is a linear curve fit through the data points indicating extensivity. This yields a value of D_{ext} for any system size N and using Eq. (2) yields a value of the natural chaotic length scale of $\xi_\delta=1.35$. It is important to point out that since $\xi_\delta>1$, incremental changes in N by adding a single lattice site allow the variation in the fractal dimension to be observed for changes in system size that are smaller than the chaotic length scale.

The deviations of the fractal dimension about extensivity ΔD are shown in Fig. 6(b) where we have used Eq. (7), and the solid line is to guide the eye. The magnitude of the deviation from extensivity for $N\leq25$ is $\sim5\%$ at its largest value and tends toward zero with increasing N. Error bars are included and, over the entire range of system sizes, have a magnitude on the order of $\sim10^{-5}$, which is three orders of magnitude smaller than the absolute values of ΔD. Due to the very small magnitude of our error bars we can discern these deviations in the fractal dimension from extensivity for all values of the system size. For the larger system sizes $40\leq N\leq50$ the variation of the deviation from extensivity is shown in Fig. 6(c).

Figure 6(b) illustrates that the variation of ΔD with N is given by an oscillating decay toward extensivity with a nonmonotonic amplitude. The previous studies exhibiting deviations from extensivity of O'Hern *et al.*[16] and Fishman and Egolf[18] both observed a rapid decay toward extensive chaos that is well described by a rapidly decaying sinusoidal function. At present we do not have a good understanding of the physical origin of the nonmonotonicity in the amplitude of our oscillating decay. This is perhaps related to the discrete spatial structure of the Lorenz-96 model. Another possibility is that the form of the deviations may reveal information regarding the symmetry of the interactions between the chaotic degrees of freedom.[18]

It is useful to separate these findings into two regimes, a small system regime where $N\leq25$ and a large system regime where $N\geq40$. The small system regime includes the onset of extensivity whereas the large systems are extensive. In a more complicated system, one would typically only have access to the deviations from extensivity for the small system sizes since the deviations are largest in this range. However, this is also the regime where one could expect pattern selection effects to be also important and complicate the results. The large system limit is expected to be less influenced by pattern selection effects and to provide a better estimate of the length scale of a chaotic degree of freedom.

Over these two regimes we find that the wavelength of the deviations varies significantly. To quantify this in the small system limit we compute the zero crossings of ΔD to estimate the wavelength of oscillation about D_{ext} given by ξ_0. For $N\leq25$ there are three wavelengths with values of (3.3, 5.3, and 1.9) that yield an average of $\xi_0=3.5$. The ratio $\xi_0/\xi_\delta=2.6$ yields that each wavelength of the deviation from extensive chaos contains approximately 2.6 chaotic degrees of freedom. The large spread in the values of the wavelengths suggests some competition with pattern selection mechanisms.

In the large system limit $N\geq40$ the data are well represented by a damped cosine wave. The solid line in Fig. 6(c) is given by $\Delta D=1.3\times10^{-3}N^{-1}\cos(2\pi N/\xi_0)$ where the wavelength is $\xi_0=2.1$ lattice spacings. The magnitude and variation of the wavelengths are smaller than what was found for the smaller systems. A similar curve fit does not represent the data for the smaller system sizes. In the large system limit the ratio $\xi_0/\xi_\delta=1.5$ yields that, on average, there are approximately 1.5 chaotic degrees of freedom per wave-

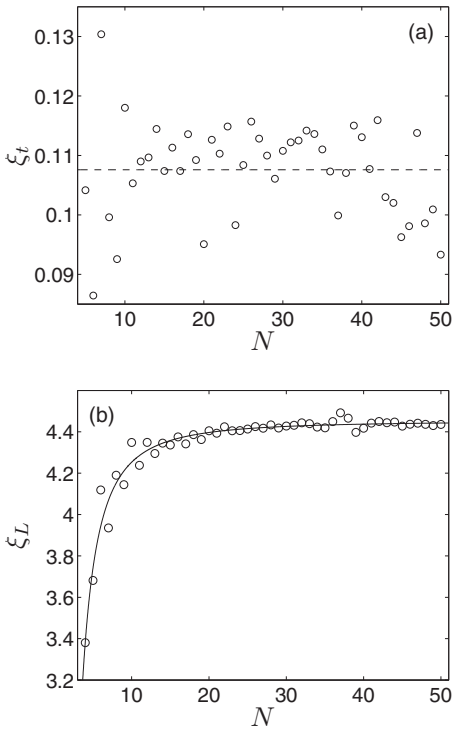

FIG. 7. The temporal and spatial characteristics of the patterns for $F=10$. (a) The variation of the average correlation time ξ_t with system size N. The dashed line is the average value of ξ_t. (b) The variation of the average pattern wavelength ξ_L with system size. The solid line is a curve fit of the form $\xi_L=4.45-13.6N^{-1.83}$.

length of the deviation from extensive chaos. As in the case of $F=5$, the length scale of the deviations from extensive chaos is consistent with the chaotic length scale suggesting that the deviations are due to the presence of additional chaotic degrees of freedom with increasing system size. Our results for small and intermediate forcing yield on the order of two chaotic degrees of freedom per wavelength of the deviation from extensivity. It is interesting to note that this is in rough agreement with what has been found for the complex Ginzburg–Landau equation although the two systems are very different.[18]

We now compute the characteristic time and length scales describing the pattern dynamics using the same diagnostics that we applied to the results where $F=5$. A motivation here is also to provide further insight into the transition between the small and large system limits in order to separate pattern selection effects from dynamical effects related to extensivity. Figure 7(a) shows the variation of the average correlation time ξ_t with N over 50 different initial conditions. The time dynamics are noisy and the correlation time has an average value of approximately $\xi_t \approx 0.11$ (indicated by the dashed line). The time dynamics are faster than what was found for $F=5$ as expected for the increased value of the forcing term.

Figure 7(b) illustrates the variation in the average wavelength of the patterns with N over the different initial conditions. The wavelength variation shows two regions of interest. For small system sizes $N \lesssim 20$ the pattern wavelength increases rapidly. For larger systems the wavelength remains relatively constant with an average value of $\xi_L \approx 4.45$. The region of increasing wavelength corresponds to system sizes where the pattern selection is affected significantly by the size of the domain. This corresponds roughly with the region where the fractal dimension is approaching extensivity in Fig. 6(b). These trends are well captured by a curve fit through the data of the form $\xi_L=4.45-13.6N^{-1.83}$ and are shown by the solid line in Fig. 7(b). The fluctuations of the wavelength about the mean value for these chaotic states yield a coefficient of variation of approximately 30%. For this reason we do not provide a comparison of the deviations of the wavelength about the average value with the deviations from extensivity as we did for $F=5$ in Fig. 4. Our space-time diagnostics indicate that in the large system limit $\xi_L \approx 3.3\xi_\delta$, indicating that a wavelength of the pattern contains, on average, 3.3 chaotic degrees of freedom. A more detailed exploration of the relationship between ξ_L and ξ_δ for increasing values of the forcing F will be explored in Sec. III B.

B. Variation of the fractal dimension with forcing

In Sec. III A we have considered the large system limit defined as the limit where the chaotic degrees of freedom are much smaller than the system size. This was achieved by holding the external forcing F fixed while the system size N was increased. This is the typical manner to study spatiotemporal chaos and has been referred to as the spatiotemporal chaos limit.[1] For example, in a Rayleigh–Bénard convection experiment this could be accomplished by holding the Rayleigh number constant while increasing the aspect ratio of the convective domain.

However, it is also possible to explore the large system limit by keeping the system size fixed while increasing the external forcing. This has been referred to as the strong driving or "strong turbulence" limit.[1] In this case, it is expected that the chaotic degrees of freedom will become smaller with increasing forcing to yield the large system limit. In a Rayleigh–Bénard convection experiment this would be accomplished by increasing the Rayleigh number in a convection domain of fixed size. It has been conjectured that the fractal dimension will also exhibit a power-law dependence with respect to the value of the forcing.[1]

We have explored this strong driving limit in the Lorenz-96 model by performing a series of simulations for increasing values of F while the system size N is held constant. We studied six values of the forcing over the range $5 \le F \le 30$. For any particular value of F we performed ten numerical simulations starting from different random initial conditions and allowed the simulation to run for 5×10^5 time units to ensure good statistics. We computed these results for five different system sizes where $15 \le N \le 35$.

It is more convenient to discuss these results using the intensive dimension density,

$$\delta_\lambda = \frac{D_\lambda}{N}. \tag{9}$$

The variation of the dimension density with external forcing is shown in Fig. 8. Each symbol is the average value of the ten simulations from different random initial conditions. The

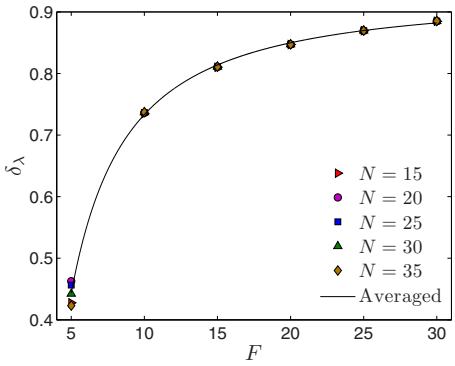

FIG. 8. (Color online) The variation of the dimension density δ_λ with the forcing F and system size N. The results are for the five different system sizes indicated in the legend. The symbols are simulation results and the solid line is a curve fit through the average value of the data given by $\delta_\lambda = 0.93 - 4.03F^{-1.32}$. Each symbol is the average value from results computed using ten different initial conditions. The magnitude of the standard deviation of these results for each symbol is $\sim 10^{-5}$.

magnitudes of the standard deviation of the results are $\sim 10^{-5}$ and have not been included as error bars due to their small magnitude.

Results for the dimension density for different values of N collapse onto a single curve given by $\delta_\lambda = 0.93 - 4.03F^{-1.32}$ and are shown by the solid line. The scatter in the results is quite small for all values of F explored with the largest deviations occurring at the smallest value of the forcing. The collapse of the data over the different system sizes explored indicates that the dynamics are in the extensive chaotic regime.

There are several interesting predictions given by the trends in the data. First is the prediction that the asymptotic value of the dimension density for external forcing of infinite magnitude saturates at a value of $\delta_\infty = 0.93 < 1$. In discussing this it is useful to note that the inverse of the dimension density is simply the natural chaotic length scale $\xi_\delta = \delta_\lambda^{-1}$. In light of this, Fig. 8 also illustrates the manner in which the chaotic length scale decreases with increasing forcing. For a spatially discrete system with N degrees of freedom the theoretical limit for the dimension density is $\delta_\lambda = 1$. This corresponds to a chaotic length scale of a single lattice spacing $\xi_\delta = 1$. Using our results for δ_∞ yields a value of $\xi_\delta = 1.08$ for the chaotic length in the limit of infinite forcing. This is in contrast to a fluid system described by partial differential equations with an infinite number of degrees of freedom. It is interesting to note that the variation of the fractal dimension with the degree of external forcing has been explored numerically for turbulent Rayleigh–Bénard convection to yield a linear dependence.[29] Second is the prediction that the dimension density vanishes at a value of $F = 3.04$ providing a threshold value for F above which one finds chaotic dynamics. We have run a series of numerical tests for values F near this threshold value to explore this further. Our results yield that this value is correct to within the precision of our calculations.

We now compare several measures of characteristic time and length scales for increasing values of the magnitude of external forcing. Both the temporal and spatial scales decrease with increasing forcing as expected. The variation of

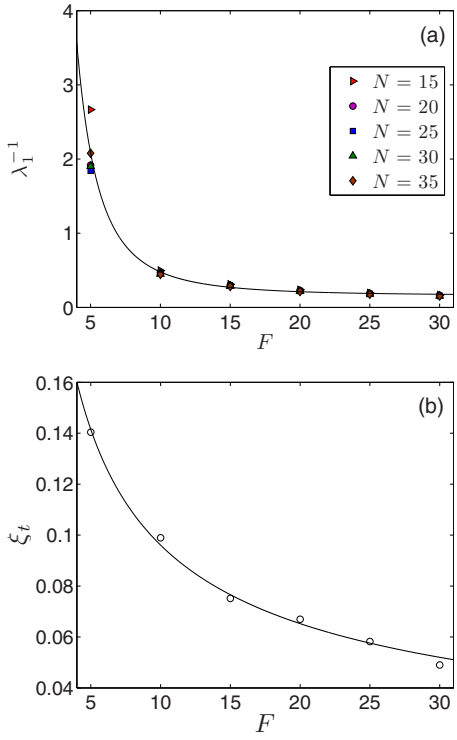

FIG. 9. (Color online) The variation of two characteristic time scales with external forcing F. (a) The variation of the inverse of the leading order Lyapunov exponent λ_1^{-1}. Data are shown for five different system sizes as indicated in the legend. The solid line is a curve fit through the data of the form $\lambda_1^{-1} = 0.158 + 123.8F^{-2.6}$. (b) The variation of the average correlation time ξ_t with F for a system size of $N = 35$. The symbols are results from simulation and the solid line is the power-law curve fit given by $\xi_t = 0.35F^{-0.56}$.

the inverse leading order Lyapunov exponent and the correlation time are shown in Fig. 9. The symbols are results from our simulations for each value of F. The value of λ_1^{-1} yields a time scale related to the predictability of the system. The solid line in Fig. 9(a) is a curve fit given by $\lambda_1^{-1} = 0.158 + 123.8F^{-2.6}$.

Figure 9(b) illustrates the variation of the average correlation time ξ_t with increased forcing and over the ten different initial conditions for a large system with $N = 35$. The solid line is given by the power-law curve fit $\xi_t = 0.35F^{-0.56}$. The fluctuations of the correlation time about the mean value over the different initial conditions are quite noisy and yield a coefficient of variation of 7.7%. In the limit of infinite forcing the average correlation time $\xi_t \approx 0$. Our results suggest that the predictability decreases faster than the correlation time indicating the possibility of at least two different time scales.

The pattern wavelength and the chaotic length scale decrease for increasing values of the magnitude of the external forcing. The variation of these length scales is shown in Fig. 10(a). The pattern wavelength is represented using square symbols and the natural chaotic length scale is represented using circle symbols. The length scales have been normalized by their magnitude at $F = 5$ to facilitate a comparison using a single plot. The normalized length scales are referred to as $\tilde{\xi}_L$ and $\tilde{\xi}_0$, respectively. The coefficient of variation over the different initial conditions for the chaotic length scale is

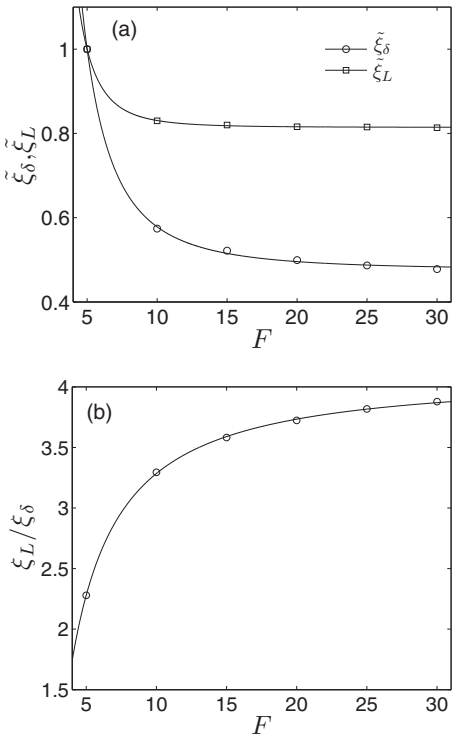

FIG. 10. The variation of two characteristic spatial scales with external forcing F for a system size of $N=35$. (a) The normalized natural chaotic length scale $\tilde{\xi}_\delta$ (circles) and the normalized pattern wavelength $\tilde{\xi}_L$ (squares). The normalization factors used are the respective values of ξ_δ and ξ_L at $F=5$. (b) ξ_L/ξ_δ yields an estimate for the number of chaotic degrees of freedom per pattern wavelength.

quite small at ~0.01%, whereas the pattern wavelength measurements are quite noisy with a coefficient of variation of ~31%.

It is clear that the natural chaotic length scale decreases more rapidly than the pattern wavelength. The ratio of these two length scales yields an estimate for the number of chaotic degrees of freedom per pattern wavelength and is shown in Fig. 10(b). For small values of the forcing there are approximately two degrees of freedom per wavelength which increases to nearly four degrees of freedom per wavelength for large values of the forcing. The separation of these two length scales suggests that for larger values of the external forcing significant contributions to the overall disorder are from subwavelength structures in the pattern dynamics. A clear signature of the subwavelength chaotic degree of freedom was not found using our spatial diagnostics. Our findings that the chaotic length scale ξ_δ is smaller than, and not correlated with, the pattern's long-range spatial order are in agreement with previous findings using the complex Ginzburg–Landau equation[30,31] and coupled map lattices.[16] A physical understanding of the chaotic length scale with respect to the spatial features of the patterns remains an open challenge and further study would be useful.

IV. CONCLUSIONS

Using a phenomenological model relevant to fluid convection and the atmosphere, we have shown that the variation of the fractal dimension with system parameters can provide physical insights into fundamental features of high-dimensional chaos. We have studied the variation of the fractal dimension in the spatiotemporal chaos and strong-driving limits in order to probe how the dynamics of a high-dimensional chaotic system vary with increasing disorder. In the spatiotemporal chaos limit we explored the cases of small external forcing ($F=5$) and intermediate external forcing ($F=10$) over a large range of system sizes. Our results yield significant deviations from extensive chaos that we use to quantify the underlying chaotic degrees of freedom. A comparison of the chaotic length scale with the wavelength of deviations from extensivity and the pattern wavelength provides estimates for the number of chaotic degrees of freedom contained per wavelength. For the parameters explored we find on the order of two chaotic degrees of freedom per wavelength of the deviation from extensivity. This is consistent with the findings of Fishman and Egolf[18] for the complex Ginzburg–Landau equation. Our results provide further evidence relating the deviations from extensivity and the chaotic length scale for a model equation with relevance to fluid systems.

For small forcing we find extensivity, on average, with alternating windows of periodic and chaotic dynamics with increasing system size over the range explored. Our results suggest the presence of competing pattern selection dynamics. This is similar to what has been found both numerically[32] and experimentally[3] in fluid systems such as Rayleigh–Bénard convection. It is possible that the dynamics would become purely extensive for very large system sizes and we have not explored this in detail. For our results, the deviations from extensive chaos exhibit significant deviations on the order of 20%. The windows of periodicity occur in nearly regular intervals of size equal to two chaotic degrees of freedom. In this parameter range we also find a correlation between the deviations from extensivity and the pattern wavelength, suggesting that the pattern wave structure contributes significantly to the chaotic dynamics.

Our results for intermediate forcing yield chaotic dynamics for all system sizes explored. We find deviations from extensivity for all system sizes including the large system limit where pattern selection effects due to the finite size of the domain are not significant. In the large system limit we find approximately 1.5 chaotic degrees of freedom per wavelength of the deviation from extensive chaos. The amplitude of the deviations from extensive chaos rapidly decays with increasing system size. For the range of system sizes approaching extensive chaos the amplitude of the oscillating decay is nonmonotonic, suggesting that there is perhaps some asymmetry in the interactions of the chaotic degrees of freedom in contrast to what has been found previously using different systems.[16,18]

In the strong driving limit we have explored the variation of the fractal dimension with increasing values of the external forcing. For the spatially discrete Lorenz-96 system there is a maximum value for the dimension density equal to unity. We find that the dimension density saturates at a value less than unity for infinite external forcing. The variation of the fractal dimension quantifies the decreasing size of a chaotic degree of freedom with increased external forcing. We

find that the chaotic length scale decreases faster than the pattern wavelength with increasing values of the external forcing. A comparison of these length scales yields that the system goes from approximately two to four chaotic degrees of freedom per wavelength of the pattern for small and large values of the external forcing, respectively. It is important to highlight that our results are in contrast to what would be found for a spatially continuous system, such as the partial differential equations that describe fluid dynamics where the fractal dimension can be infinite.

If one considers only the space-time diagnostics of the correlation time and pattern wavelength the results exhibit significant fluctuations despite the use of very long-time simulations for numerous initial conditions. This is in contrast to what is found when using the fractal dimension and suggests the possibility of features of the dynamics that have yet to be quantified in detail. Clearly identifying such features, and relating them to experimentally accessible quantities, remains an important open challenge in the characterization of systems driven far-from-equilibrium. It is anticipated that our results will be useful in guiding future efforts to explore the extensive chaos of experimentally accessible systems.

ACKNOWLEDGMENTS

The computations were conducted using the resources of the Advanced Research Computing center at Virginia Tech and the research was supported by NSF Grant No. CBET-0747727.

[1]M. C. Cross and P. C. Hohenberg, "Pattern formation outside of equilibrium," Rev. Mod. Phys. **65**, 851 (1993).
[2]E. N. Lorenz, "The predictability of a flow which possesses many scales of motion," Tellus **XXI**, 289 (1968).
[3]E. Bodenschatz, W. Pesch, and G. Ahlers, "Recent developments in Rayleigh-Bénard convection," Annu. Rev. Fluid Mech. **32**, 709 (2000).
[4]M. A. Bees and N. A. Hill, "Wavelengths of bioconvection patterns," J. Exp. Biol. **200**, 1515 (1997).
[5]M. Bär and M. Eiswirth, "Turbulence due to spiral breakup in a continuous medium," Phys. Rev. E **48**, R1635 (1993).
[6]C. R. Nugent, W. M. Quarles, and T. H. Solomon, "Experimental studies of pattern formation in a reaction-advection-diffusion system," Phys. Rev. Lett. **93**, 218301 (2004).
[7]H. D. I. Abarbanel, *Analysis of Observed Chaotic Data* (Springer, New York, 1996).
[8]S. Wiggins, *Introduction to Applied Nonlinear Dynamical Systems and Chaos* (Springer, New York, 2003).
[9]E. N. Lorenz, "Deterministic nonperiodic flow," J. Atmos. Sci. **20**, 130 (1963).
[10]J. C. Robinson, "Finite-dimensional behavior in dissipative partial differential equations," Chaos **5**, 330 (1995).
[11]H. Yang, K. A. Takeuchi, F. Ginelli, H. Chatè, and G. Radons, "Hyperbolicity and the effective dimension of spatially extended dissipative systems," Phys. Rev. Lett. **102**, 074102 (2009).
[12]E. Ott, *Chaos in Dynamical Systems* (Cambridge University Press, New York, 1993).
[13]J.-P. Eckmann and D. Ruelle, "Ergodic theory of chaos and strange attractors," Rev. Mod. Phys. **57**, 617 (1985).
[14]J. D. Farmer, E. Ott, and J. A. Yorke, "The dimension of chaotic attractors," Physica D **7**, 153 (1983).
[15]D. Ruelle, "Large volume limit of the distribution of characteristic exponents in turbulence," Commun. Math. Phys. **87**, 287 (1982).
[16]C. S. O'Hern, D. A. Egolf, and H. S. Greenside, "Lyapunov spectral analysis of a nonequilibrium Ising-like transition," Phys. Rev. E **53**, 3374 (1996).
[17]P. Manneville, "Microscopic modeling of turbulent flows," Lect. Notes Phys. **230**, 319 (1985).
[18]M. P. Fishman and D. A. Egolf, "Revealing the building blocks of spatiotemporal chaos: Deviations from extensivity," Phys. Rev. Lett. **96**, 054103 (2006).
[19]S. Tajima and H. S. Greenside, "Microextensive chaos of a spatially extended system," Phys. Rev. E **66**, 017205 (2002).
[20]H. W. Xi, R. Toral, J. D. Gunton, and M. I. Tribelsky, "Extensive chaos in the Nikolaevskii model," Phys. Rev. E **62**, R17 (2000).
[21]D. A. Egolf, I. V. Melnikov, W. Pesch, and R. E. Ecke, "Mechanisms of extensive spatiotemporal chaos in Rayleigh-Bénard convection," Nature (London) **404**, 733 (2000).
[22]M. R. Paul, M. I. Einarsson, P. F. Fischer, and M. C. Cross, "Extensive chaos in Rayleigh-Bénard convection," Phys. Rev. E **75**, 045203 (2007).
[23]E. N. Lorenz, in *Proceedings of the Seminar on Predictability*, Vol. I, ECWF Seminar, edited by T. Palmer (ECMWF, Reading, UK, 1996), pp. 1–18.
[24]E. N. Lorenz and K. A. Emanuel, "Optimal sites for supplementary weather observations: Simulation with a small model," J. Atmos. Sci. **55**, 399 (1998).
[25]G. Boffetta, M. Cencini, M. Falcioni, and A. Vulpiani, "Predictability: A way to characterize complexity," Phys. Rep. **356**, 367 (2002).
[26]E. Ott, B. R. Hunt, I. Szunyogh, A. V. Zimin, E. J. Kostelich, E. Kalnay, D. J. Patil, and J. A. Yorke, "A local ensemble Kalman filter for atmospheric data assimilation," Tellus **56**, 415 (2004).
[27]D. Pazó, I. G. Szendro, J. López, and M. A. Rodríguez, "Structure of characteristic Lyapunov vectors in spatiotemporal chaos," Phys. Rev. E **78**, 016209 (2008).
[28]A. Wolf, J. B. Swift, H. L. Swinney, and J. A. Vastano, "Determining Lyapunov exponents from a time series," Physica D **16**, 285 (1985).
[29]L. Sirovich and A. E. Deane, "A computational study of Rayleigh-Bénard convection. Part 2. Dimension considerations," J. Fluid Mech. **222**, 251 (1991).
[30]D. A. Egolf and H. S. Greenside, "Relation between fractal dimension and spatial correlation length for extensive chaos," Nature (London) **369**, 129 (1994).
[31]D. A. Egolf and H. S. Greenside, "Characterization of the transition from defect to phase turbulence," Phys. Rev. Lett. **74**, 1751 (1995).
[32]M. R. Paul, M. C. Cross, P. F. Fischer, and H. S. Greenside, "Power-law behavior of power spectra in low Prandtl number Rayleigh-Bénard convection," Phys. Rev. Lett. **87**, 154501 (2001).